Colloids and Surfaces B: Biointerfaces 165 (2018) 150–157

Contents lists available at ScienceDirect

Colloids and Surfaces B: Biointerfaces

journal homepage: www.elsevier.com/locate/colsurfb

Biocatalysts based on nanozeolite-enzyme complexes: Effects of alkoxysilane surface functionalization and biofuel production using microalgae lipids feedstock

Adriano de Vasconcellos[a], Alex Henrique Miller[a], Donato A.G. Aranda[b], José Geraldo Nery[a,*]

[a] Laboratory for Clean Energy Technology (LACET), Physics Department, São Paulo State University–UNESP, Campus de São José do Rio Preto, SP, 15054-000, Brazil

[b] Greentec Laboratory, School of Chemistry, Federal University of Rio de Janeiro, RJ, 21941-972, Brazil

ARTICLE INFO

Article history:
Received 20 September 2017
Received in revised form 16 January 2018
Accepted 13 February 2018
Available online 14 February 2018

Keywords:
Nanozeolite surface chemical modulation
Zeolite-enzyme surface interaction
Non-edible lipid feedstocks
Biofuels
Biomass

ABSTRACT

Nanozeolites with different crystallographic structures (Nano/TS1, Nano/GIS, Nano/LTA, Nano/BEA, Nano/X, and Nano-X/Ni), functionalized with (3-aminopropyl)trimethoxysilane (APTMS) and crosslinked with glutaraldehyde (GA), were studied as solid supports for *Thermomyces lanuginosus* lipase (TLL) immobilization. Physicochemical characterizations of the surface-functionalized nanozeolites and nanozeolite-enzyme complexes were performed using XRD, SEM, AFM, ATR-FTIR, and zeta potential measurements. The experimental enzymatic activity results indicated that the nanozeolitic supports functionalized with APTMS and GA immobilized larger amounts of enzymes and provided higher enzymatic activities, compared to unfunctionalized supports. Correlations were observed among the nanozeolite surface charges, the enzyme immobilization efficiencies, and the biocatalyst activities. The catalytic performance and reusability of these enzyme-nanozeolite complexes were evaluated in the ethanolysis transesterification of microalgae oil to fatty acid ethyl esters (FAEEs). TLL immobilized on the nanozeolite supports functionalized with APTMS and GA provided the most efficient biocatalysis, with FAEEs yields above 93% and stability during five reaction cycles. Lower FAEEs yields and poorer catalytic stability were found for nanozeolite-enzyme complexes prepared only by physical adsorption. The findings indicated the viability of designing highly efficient biocatalysts for biofuel production by means of chemical modulation of nanozeolite surfaces. The high biocatalyst catalytic efficiency observed in ethanolysis reactions using a lipid feedstock that does not compete with food production is an advantage that should encourage the industrial application of these biocatalysts.

1. Introduction

The production of liquid biofuels from biomass is one of the options available to help meet the increasing energy demands caused by the life styles in industrialized countries and by the rapid economic growth of populous developing countries. This high energy demand currently mainly relies on fossil fuels, but environmental concerns and the depletion of fossil fuel resources have stimulated the search for alternative renewable fuels that are environmentally benign and sustainable. Biodiesel can play a major role in this challenge of finding a viable alternative for the replacement of the fossil fuels used in the transportation sector [1,2].

The task of searching for new sources of clean and renewable energy is not straightforward and needs to consider various factors including the economic viability of non-edible biomass sources, the development of new catalysts, and the use of low cost processing technologies [3]. First generation biodiesels are produced from biomass feedstocks consisting of food and oil crops, using conventional chemical technologies [4,5], and a large proportion (95%) of biodiesel production still relies on edible oil sources [6]. The use of edible feedstocks has raised many ethical and economic questions, due to its negative impacts on global food markets and food security [7]. Alternative biomass sources such as non-food crops [8], animal fats [9,10], and waste cooking oils [11,12] are employed in the production of second generation biodiesel, but the use of

* Corresponding author at: Rua Cristóvão Colombo 2265, São José do Rio Preto, SP, 15054-000, Brazil.
E-mail address: nery@ibilce.unesp.br (J.G. Nery).

https://doi.org/10.1016/j.colsurfb.2018.02.029
0927-7765/

Table 1
Synthesis parameters of the nanozeolite materials.

Sample	Silica Source	Aluminum or Titanium Source	Cation Type	Synthesis time (h)	Temperature (°C)	Ref.
Nano-TS1	TEOS	TBOT	TPA^+	24	100	[45]
Nano-GIS	TEOS	AlIso	TMA^+	312	100	[46]
Nano-BEA	Silica Fumed	TEA	TEA^+	120	140	[47]
Nano-LTA	Ludox	AlIso	TMA^+	24	60	[48]
Nano-X	Silica Fumed	Sodium aluminate	Na^+	48	60	[49]

TEOS = tetraethylorthosilicate; TBOT = tetrabutylorthotitanate; AlIso = aluminumisopropoxide; TMA^+ = tetramethylammonium; TEA^+ = tetraethylammonium, TPA^+ = tetrapropylammonium; Ludox = aqueoussilicasolution (Ludox HS-30, 30 wt%).

these feedstocks has drawbacks related to the processing costs in large-scale commercial operations [13,14].

The third generation of biodiesel proposes the use of microalgae as an alternative biomass feedstock [15]. This is considered by experts in the energy field as a technically feasible alternative capable of overcoming the main difficulties associated with the feedstocks employed in first and second generation biodiesel production [16].

Heterotrophic and photoautotrophic microalgae are viable candidates for biodiesel production, due to their high photosynthetic efficiency, rapid formation of large amounts of biomass, high lipid contents that can be equivalent to that of soybean, and faster large-scale growth compared to other energy crops [17,18]. In addition, some heterotrophic microalgae can be cultivated in the absence of light, using a non-photosynthetic process, while others can be produced during fermentation of a reduced carbon source [19]. For practical and economic reasons, heterotrophic microalgae have several advantages over photoautotrophic organisms, including faster biomass accumulation under controlled conditions that decrease the likelihood of common problems affecting large-scale microalgae cultivation, such as variations in light intensity and the available carbon source [20]. Another advantage of heterotrophic microalgae is that genetically modified strains are capable of producing lipid yields higher than 80%, while photoautotrophic cultures of native algae yield only 20–50% of lipids [21,22]. Although heterotrophic microalgae are incapable of capturing CO_2 emissions, the overall heterotrophic process is cyclic, because the initial organic substrates are produced by photosynthetic plants [23].

There are four different catalytic routes in triacylglycerides transesterification reactions: (i) base-catalyzed processes, (ii) acid-catalyzed processes, (iii) enzyme-catalyzed processes, and (iv) use of supercritical conditions. The advantages and disadvantages of these different routes have been discussed in several review papers [24,25]. Currently, industrial biodiesel production mainly employs the homogeneous base-catalyzed process, using sodium hydroxide (NaOH), potassium hydroxide (KOH), sodium methoxide ($NaOCH_3$), or sodium ethoxide ($NaOCH_2CH_3$) as the catalyst [26]. However, there are several drawbacks associated with this process, especially when low quality feedstocks with high contents of water and free fatty acids (FFAs) are used. In this case, the use of base catalysts increases the energy cost and the likelihood of soap and emulsion formation, which can lead to the generation of large amounts of wastewater during the processes of cleaning and separation of the glycerol (byproduct) and biodiesel (product) [26,27]. Hence, in order to overcome these drawbacks, alternative and more sustainable catalytic routes for biodiesel production are being sought.

The use of lipases as catalysts in biodiesel production is an attractive option, due to their higher specificity for the transesterification of triacylglycerides to fatty acid methyl esters (FAMEs) or fatty acid ethyl esters (FAEEs), compared to the conventional chemical catalysts employed in industrial biodiesel production. Enzymes exhibit greater selectivity and higher catalytic activity in transesterification reactions under mild operational conditions (25–60 °C), compared to homogeneous basic catalysts [28]. In addition, lipases can catalyze the transesterification of raw materials that contain high levels of FAAs and water, with decreased risk of soap and emulsion formation [28]. However, despite all the advantages of the enzymatic process, there are important issues that hinder its use in industrial scale processes for biodiesel production. These include: a) the high costs of enzymes, b) problems in separating the product from the reaction medium, c) difficulty in recovering and reusing enzymes, and d) deactivation of the active sites of enzymes by the substrates (short-chain alcohols such as methanol and ethanol) [29] and by the glycerol byproduct [30]. One way to overcome these obstacles is to immobilize the enzymes on solid carriers [31,32]. The selection of suitable solid supports needs to consider aspects including the overall enzymatic activity of the immobilized enzyme, the cost of the immobilization procedure, identification of the best operating conditions in order to avoid enzyme inactivation, and the ability to regenerate and reuse the enzyme-support complex [33].

Zeolites [34,35] and enzymes [36,37] are capable of catalyzing the transesterification of triacylglycerides into FAEEs or FAMEs. These different classes of materials have inherent characteristics that determine the yield of the desired final product under different experimental conditions [38]. Nonetheless, the combination of these different classes of catalysts can result in zeolite-enzyme complexes that offer outstanding catalytic performance [38].

Nanozeolites are hydrophobic supports with high external surface areas, whose high dispersibility in both aqueous solutions and organic media allows better access of the enzymes to the substrate. This also acts to reduce the adsorption of glycerol molecules onto the biocatalyst microenvironment, and electrostatic and hydrophobic interactions within the zeolite-enzyme system contribute to its stability. Several mechanisms have been proposed for the immobilization of lipase on zeolitic supports: a) electrostatic and acid-base linkages [38], b) formation of strong enzyme-support ionic interactions [39–41], and c) covalent bonding of lipases to the zeolite surface by functionalization of the zeolite surface with alkoxysilane, followed by crosslinking with glutaraldehyde [42]. Among the available immobilization methods, covalent attachment is the most effective in terms of enhancing uptake of the enzyme and its retention on the solid support. The covalent bonding of enzymes to solid matrices can improve the feasibility of using enzymes in industrial applications, considering aspects such as denaturation of the enzyme by heat or organic solvents, pH control of the medium, stability during storage, and reduction of leaching [43].

Studies of biocatalysts based on nanozeolite-lipase complexes for the purpose of biodiesel production have not been widely reported in the literature. Transesterification of palm oil to FAEEs using lipases of *Thermomyces lanuginosus* (TLL) and *Rhizomucor miehei* (RML) immobilized on nanosized NaX zeolite (FAU) ion-exchanged with different transition metals has shown positive results. This has encouraged further synthetic and catalytic studies of enzyme-nanozeolite complexes with supports derived from different zeolite structures, and their application in the catalytic conversion of different non-edible biomasses to biodiesel [44]. Nev-

ertheless, careful analysis of the literature shows that there have been no systematic studies describing the chemical modulation of nanozeolite support surfaces using chemical modifiers such as the alkoxysilane molecule (3-aminopropyl)trimethoxysilane (APTMS), with crosslinking using glutaraldehyde (GA), and the effects on the nanozeolite-enzyme complexes. In order to address this lack of information, the present research work was undertaken with the aim of answering the following questions: a) What are the enzymatic and catalytic performances of *Thermomyces lanuginosus* (TLL) lipases immobilized on different nanosized zeolites (TS1, GIS, BEA, LTA, NaX, and NaX-Ni) previously functionalized with APTMS and crosslinked with GA? b) Are these biocatalysts effective in the transesterification of oil from the microalga *Prototheca moriformis* (a non-edible lipid feedstock source) into FAEEs using the ethanolysis route? c) Do the functionalized biocatalysts provide better catalytic results than unfunctionalized biocatalysts, especially in terms of the FAEEs yield and biocatalyst stability? The experimental results obtained in the search to answer these questions are presented and discussed here, with evaluation of the potential applications of these biocatalysts in the biofuels industry.

2. Experimental section

2.1. Materials

Flavorless high-oleic (>80%) oil extracted from the genetically modified heterotrophic algal strain *Prototheca moriformis* S2532 was obtained from Solazyme (Campinas, São Paulo, Brazil). The oil consisted of triglycerides (95%), small amounts of diglycerides (<5%), trace amounts of monoglycerides (<0.5%), and small quantities of fatty acid (1%). Ethanol (99.8%), phosphate buffer, gum arabic, inorganic salts, glutaraldehyde, (3-aminopropyl)trimethoxysilane ($H_2N(CH_2)_3Si(OCH_3)_3$) (APTMS), organic bases, and enzymes were purchased from Sigma-Aldrich and were used as received, without further purification. The lipase enzyme employed in this work was Lipolase 100 L from *T. lanuginosus*. This enzyme consisted of purified 1,3-specific lipases (EC 3.1.1.3) produced by submerged fermentation of a genetically modified strain of *Aspergillus oryzae*.

2.2. Synthesis of nanozeolites

The conditions used in the syntheses of the nanozeolites (TS1, GIS, LTA, BEA, and NaX) prepared in this study are summarized in Table 1. The final gel molar compositions of the nanozeolites were as follows: TS1 (0.36 TPAOH: 0.06TiO_2: 1.00SiO_2: 16.2H_2O: 4 EtOH: 0.24 BuOH) [45]; GIS (1 Al_2O_3: 4.17 SiO_2: 2.39 TMA_2O: 253 H_2O) [46]; BEA (0.36 TPAOH: 0.06TiO_2: 1.00SiO_2: 16.2H_2O: 4 EtOH: 0.24 BuOH) [47]; LTA (0.4 Na_2O:1.9 Al_2O_3: 14.0 $(TMA)_2O$: 11.9 SiO_2:700 H_2O) [48]; NaX (5.5 Na_2O:1.0 Al_2O_3:4.0 SiO_2:190 H_2O) [49].

In a typical synthesis procedure, an aluminosilicate gel was prepared by mixing together freshly prepared aluminate and silicate solutions (or titanate and silicate solutions, in the case of TS1), following experimental procedures adapted from the literature [45–49]. The nanocrystals were cooled to room temperature and were then recovered by centrifugation (Hitachi Koki himac CR22N High-Speed Refrigerated Centrifuge), washed with deionized water until reaching pH <8, and dried at room temperature for 24 h. These samples were denoted U-Nano/TS1, U-Nano/GIS, U-Nano/LTA, U-Nano/BEA, and U-Nano-X (where U stands for unfunctionalized nanozeolite).

2.3. Ion exchange of the nanozeolitic supports

Prior to enzyme immobilization, the U-Nano-X/Na material was used in ion exchange experiments in which the sodium cations were replaced with nickel ions. These experiments were only performed with U-Nano-X/Na, because some of the other nanozeolites presented low aluminum contents (see the results of the ICP-AES analyses of U-Nano/TS1 and U-Nano/BEA),while others (U-Nano/LTA and U-Nano/GIS) did not retain their structures under the ion exchange conditions employed. The procedure was carried out as follows: 1 g of U-Nano-X/Na was transferred to a Teflon-lined digestion reactor (Parr Instruments), together with 30 mL of 0.5 mol L^{-1} $NiSO_4$ solution. The ion exchange reaction was allowed to proceed for 72 h at 60 °C, followed by centrifugation of the mixture at 13,400*g*, washing of the solid product three times with distilled water, and drying at room temperature. This ion-exchanged derivative was designated U-Nano-X/Ni.

2.4. Functionalization of the nanozeolitic supports

2.4.1. Functionalization of the nanozeolite surfaces with APTMS

Prior to the functionalization, all the as-synthesized nanozeolites (U-Nano/TS1, U-Nano/GIS, U-Nano/LTA, and U-Nano/BEA) were thermally treated in order to remove the organic templates used in their syntheses. The samples were heated in an air stream at 550 °C, using the following temperature ramps: 25–100 °C (1 h), 100–150 °C (30 min), 150–200 °C (30 min), and 200–550 °C (3 h). The samples were kept at the final temperature of 550 °C for 3 h. The functionalization reactions with APTMS were performed according to the method described by Plueddemann et al. [50] and updated by Li et al. [51]. The procedure involved three steps: (1) stirring a mixture of dichloromethane (30 mL) + APTMS (2 mL) + zeolite (1 g) for 16 h at room temperature; (2) centrifugation at 13,400x*g* and washing the solid samples three times with methanol to remove the unreacted APTMS; (3) drying the modified zeolite for 12 h at 60 °C under vacuum. These alkoxysilane functionalized nanozeolites were denoted N-Nano/TS1, N-Nano/GIS, N-Nano/LTA, N-Nano/BEA, N-Nano/X, and N-Nano-X/Ni (where N stands for the APTMS functionalized nanozeolite).

2.4.2. Crosslinking of the APTMS functionalized nanozeolites with GA

The APTMS functionalized nanozeolites were crosslinked with glutaraldehyde (GA) as described in the literature [52]. A typical experiment was performed as follows: 1 g of the APTMS-nanozeolite was mixed with 30 mL of an aqueous 2.5 wt.% GA solution and stirred for 24 h at room temperature. The suspension turned yellow immediately after mixing, then orange, and finally red. The GA-functionalized nanozeolite was collected by centrifugation (13,400*g*) and the solid product was washed three times with distilled water, dried at room temperature, and stored under vacuum in order to prevent oxidation. There covered samples were denoted NG-Nano/TS1, NG-Nano/GIS, NG-Nano/LTA, NG-Nano/BEA, NG-Nano/X, and NG-Nano-X/Ni (where G stands for the APTMS-functionalized nanozeolite crosslinked with glutaraldehyde). Experimental details of the lipase immobilization on the nanozeolitic supports and determination of the enzymatic hydrolytic activities of the immobilized enzymes (measured using a titrimetric method) are provided in the Supplementary materials section of this journal.

The nanozeolite-enzyme complexes were named according to the nomenclatures of their preceding functionalized derivatives and the as-synthesized nanozeolites. The nanozeolite-enzyme complexes derived from *T. lanuginosus* lipase were designated U-Nano/TS1-TLL, U-Nano/GIS-TLL, U-Nano/LTA-TLL, U-Nano/BEA-TLL, U-Nano/X-TLL, and U-Nano-X/Ni-TLL. The nanozeolite-enzyme complexes derived from the APTMS-functionalized supports were designated N-Nano/TS1-TLL, N-Nano/GIS-TLL, N-Nano/LTA-TLL, N-Nano/BEA-TLL, N-Nano/X-TLL, and N-Nano-X/Ni-TLL. The nanozeolite-enzyme complexes derived from the nanozeolitic supports crosslinked with glutaraldehyde were des-

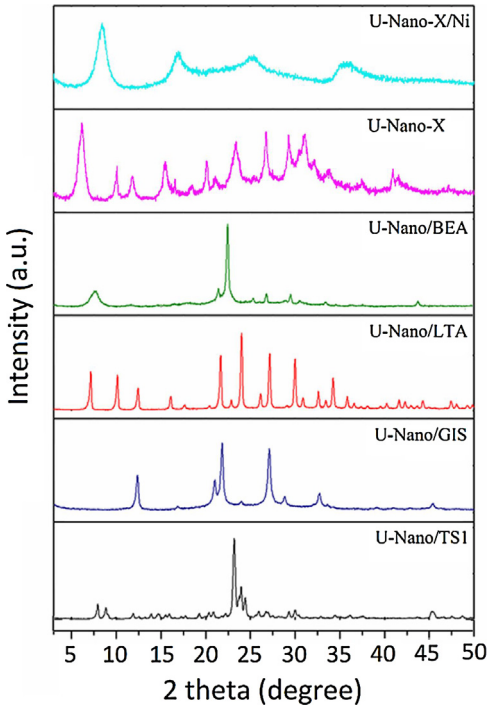

Fig. 1. XRD patterns of the as made nanozeolites.

ignated NG-Nano/TS1-TLL, NG-Nano/GIS-TLL, NG-Nano/LTA-TLL, NG-Nano/BEA-TLL, NG-Nano/X-TLL,and NG-Nano-X/Ni-TLL.

2.5. Physicochemical characterization of the as-synthesized nanozeolites and the nanozeolite-enzyme complexes

The prepared materials described above were characterized using XRD and SEM. The XRD analyses were performed with a MiniFlex II instrument (Rigaku, Tokyo, Japan) equipped with a rotating anode source with flat-plate Bragg-Brentano geometry and a graphite monochromator, operating at 40 kV and 40 mA, with Cu Kα radiation (wavelength = 1.5418 Å). The powder diffraction patterns were recorded in the 2θ range from 3 to 50°, with scanning at a goniometer rate of 2° min^{-1}. SEM images were recorded using an XL30 FEG instrument (FEI/Philips), with deposition of a thin coating of gold onto the samples prior to the analyses. FTIR spectra were acquired using a PerkinElmer Frontier FTIR spectrometer equipped with an ATR accessory. The samples were scanned 64 times between 4000 and 400 cm^{-1}, at a resolution of 4 cm^{-1}. Elemental chemical analyses of the nanozeolitic supports were performed using inductively coupled plasma atomic emission spectroscopy (ICP-AES) at the Chemical Analysis Laboratory Facility of Sao Paulo University. Atomic force microscopy (AFM) analyses were performed at the Brazilian National Laboratory of Nanotechnology (LNNano, Campinas), using a Dimension 3000 scanning probe microscope (SPM) equipped with a NanoScopeIIIa SMP controller (Digital Instruments Inc.). TESP tapping mode AFM images were acquired in ambient air using etched silicon probes. Zeta potential measurements were performed with a Zetasizer Nano ZS90 system (Malvern Instruments, Worcestershire, U.K.), using 1–2% (by weight) suspensions of the nanozeolites in deionized water. The samples were sonicated for 30 min before being transferred to disposable zeta potential cells for the measurements. Chromatographic analyses were performed with a PerkinElmer Clarus 580 gas chromatograph equipped with a flame ionization detector (GC-FID). Experimental details of these analyses are provided in the Supplementary material section of this journal.

Table 2
Chemical compositions of nanozeolitic supports obtained by ICP-OES.

Sample	SiO_2 (%)	Al_2O_3 (%)	Na_2O (%)	TiO_2(%)	NiO(%)
Nano-TS1	81.65	–	<0.01	1.10	–
Nano-GIS	42.73	16.60	1.27	–	–
Nano-LTA	37.42	24.98	11.69	–	–
Nano-BEA	81.92	3.69	<0.03	–	–
Nano-X/Na	33.23	20.84	13.97	–	–
Nano-X/Ni	18.23	12.83	0.12	–	14.88

2.6. Syntheses of FAEEs

The transesterification reactions of the high-oleic heterotrophic microalgae oil to biodiesel were performed with three different catalyst groups: (i) the as-synthesized nanozeolite-enzyme complexes (U-Nano/TS1-TLL, U-Nano/GIS-TLL, U-Nano/LTA-TLL, U-Nano/BEA-TLL, U-Nano/X-TLL, and U-Nano-X/Ni-TLL); (ii) the nanozeolite-enzyme complexes derived from the amino-functionalized supports (N-Nano/TS1-TLL, N-Nano/GIS-TLL, N-Nano/LTA-TLL, N-Nano/BEA-TLL, N-Nano/X-TLL, and N-Nano-X/Ni-TLL); and (iii) the nanozeolite-enzyme complexes derived from the glutaraldehyde-activated supports (NG-Nano/TS1-TLL, NG-Nano/GIS-TLL, NG-Nano/LTA-TLL, NG-Nano/BEA-TLL, NG-Nano/X-TLL,and NG-Nano-X/Ni-TLL).

Several experiments were performed in order to establish appropriate reaction conditions that would allow comparison among the performances of the three catalyst groups. Transesterification reactions catalyzed by the different nanozeolite-enzyme complexes were performed at 40 °C, using an oil:ethanol ratio of 1:5, with slow addition of ethanol in order to avoid inactivation of the catalysts. After a reaction time of 48 h, the product (biodiesel) and byproduct (glycerol) were separated by centrifugation at 13,400*g*. The progress of the transesterification reactions was followed using thin layer chromatography (TLC), according to the procedure described by Yang et al. [53]. At predetermined time intervals, a small volume (100 μL) of the reaction mixture was collected and mixed with 500 μL of hexane for 2 min. After separation by centrifugation, 3 μL of the upper layer was applied to a silica gel plate. A solution of hexane/ethyl acetate/acetic acid (90:10:1) was used as the developing solvent and iodine was used as the color reagent.

3. Results and discussion

The XRD results (Fig. 1) revealed successful synthesis of Nano/TS1, Nano/GIS, Nano/LTA, Nano/BEA, Nano-X/Na, and Nano-X/Na ion-exchanged with nickel (Nano-X/Ni). In the case of Nano/TS1, most of the original Bragg reflections matched the XRD pattern reported for the MFI structure [45,54]. The XRD pattern of as-synthesized Nano/GIS with the Bragg reflections at 2θ of 12.4°, 21.7°, and 27.2° corresponds to the typical reflections of a tetrahedral GIS zeolite [46]. The XRD patterns of zeolites LTA and BEA (Fig. 1) indicated that the materials were obtained as pure crystalline phases [47,48,55]. The XRD data for the Nano-X/Na zeolite were also indicative of a pure zeolite with faujasite topology, without the presence of organic templates or structure-directing agents (SDAs) [49,56]. However, ion exchange of the as-synthesized Nano-X/Na zeolite with nickel (producing Nano-X/Ni) resulted in a drastic change in the crystallographic structure (Fig. 1).

The chemical compositions of the as-synthesized nanozeolites were determined by ICP-AES analyses and are summarized in Table 2. The SiO_2: TiO_2 ratio of 74.2 obtained for Nano/TS1 was in agreement with the results reported in previous studies [45,54]. The SiO_2:Al_2O_3 ratios observed for the aluminosilicates Nano/BEA (22.2), Nano/GIS (2.57), Nano/LTA (1.49), and Nano/X (1.59) also agreed with the ratios reported elsewhere [46–48,56]. The high

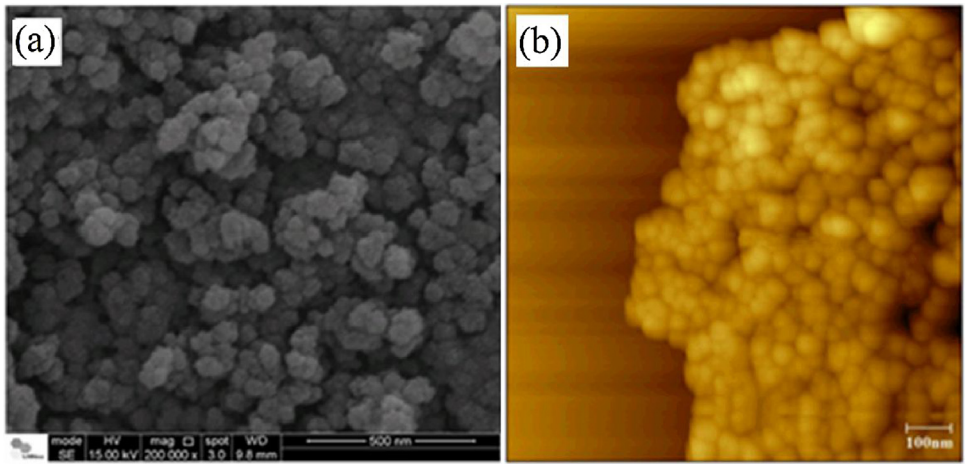

Fig. 2. Microscopy data for the U-Nano-BEA,SEM (a) and AFM (b).

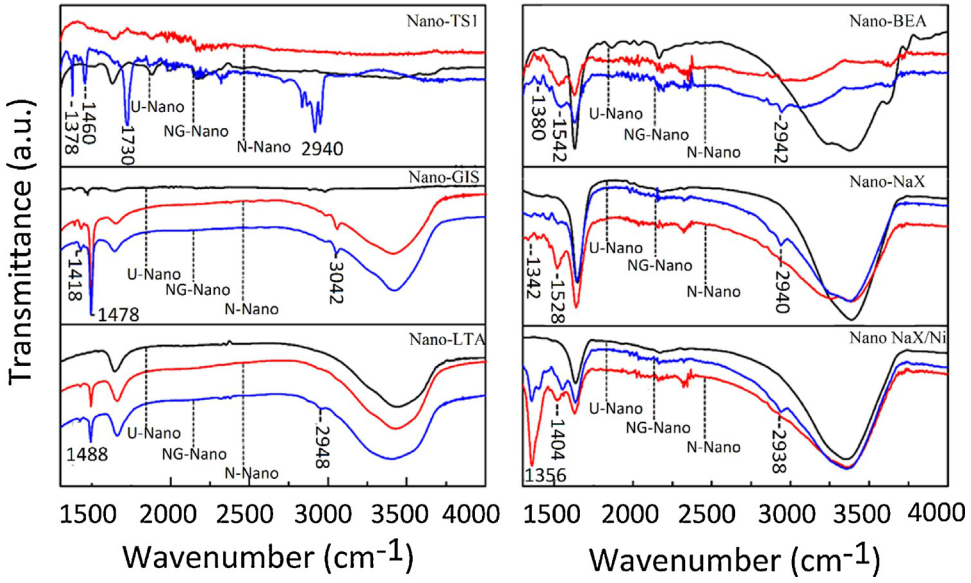

Fig. 3. The FTIR spectra of as made nanozeolite, amine-terminated surface nanozeolite and glutaraldehyde amino crosslinking nanozeolite.

SiO_2:Al_2O_3 ratio for Nano/BEA was indicative of the predominance of Si—O—Si linkages, while the lower values for Nano/LTA and Nano/X reflected higher amounts of aluminum in the crystallographic structures, which had direct effects in the nickel ion exchange experiments.

The SEM and AFM data for Nano/TS1, Nano/GIS, and Nano/LTA, are shown in the Supplementary materials section of this journal. In general TS1, GIS, and LTA nanozeolites presented spherical morphology, with sizes in the range 50–180 nm and. the homogeneous shapes and diameters of the nanocrystals were in accordance with other results reported in the literature [45,46,48].

The morphology of Nano/BEA (Fig. 2) was characterized by agglomerates of nanocrystals, typical of nanozeolite beta [47], with the SEM and AFM images revealing crystals around 50 nm in size. The SEM and AFM images of Nano-X/Na (Supplementary materials section) showed the presence of large nanoparticle aggregates approximately 250 nm in size, composed of smaller particles with sizes in the range 20–100 nm [49,56]. In contrast, the SEM and AFM images for Nano-X/Ni showed the presence of crystal aggregates with no specific morphology, indicating that the ion exchange process damaged the original Nano/X structure.

ATR-FTIR spectra of the as-synthesized and functionalized nanozeolites were measured in the range 400–4000 cm^{-1}. According to the literature, the infrared spectroscopy spectra for aluminosilicate zeolites can be divided into two distinct regions, corresponding to the skeletal IR spectrum(at 1600–500 cm^{-1}) and the surface hydroxyl groups (at 4000–1500 cm^{-1}) [57]. Analyses of the skeletal regions (1600–500 cm^{-1}) of the ATR-FTIR spectra of the unfunctionalized U-Nano/TS1, U-Nano/GIS, U-Nano/LTA, U-Nano/BEA, and U-Nano-X/Na zeolites (see Supplementary materials section) showed that the absorption bands for the as-synthesized nanozeolite structures were in agreement with the values reported in the literature. However, for U-Nano-X/Ni, the absorption bands in the skeletal region (at 425, 552, 795, 912, and 1064 cm^{-1}) were shifted from the positions expected for aluminosilicates. This was a clear indication that the ion exchange treatment affected the original Nano-X/Na framework, corroborating the XRD results.

The ATR-FTIR spectra of the functionalized nanozeolites (Fig. 3) revealed two absorption bands in the region 1350–1460 cm^{-1}, which could be attributed to the bending of (CH)—R—CH_3 and the methyl groups (—CH_3) of glutaraldehyde [58]. Absorption bands at 1530 and 1750 cm^{-1} corresponded to the stretching of C=O

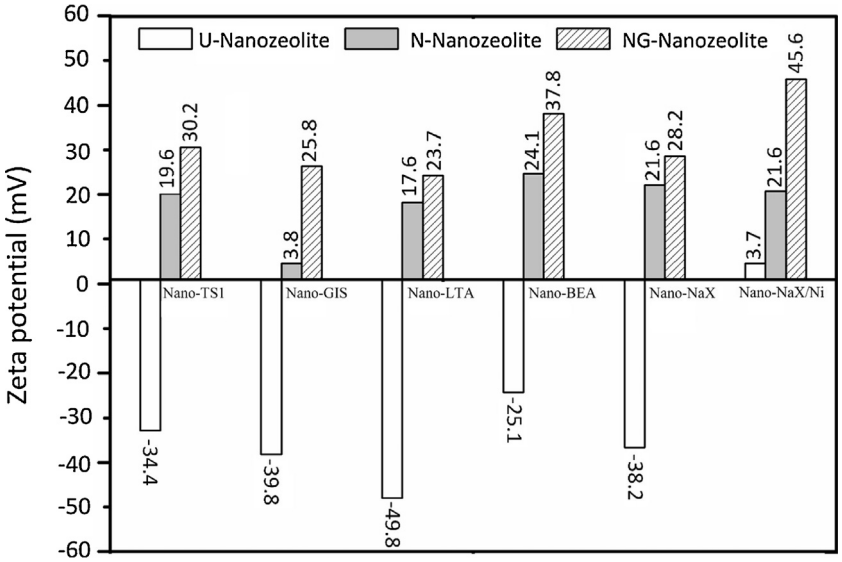

Fig. 4. Zeta potential for as made nanozeolite, amine-terminated surface nanozeolite and glutaraldehyde amino crosslinking nanozeolite.

and C=N bonds, evidencing crosslinking of the GA group, while bands at 2950 and 2880 cm^{-1} corresponded to aldehyde C—H and alkyl C—H stretching vibrations, respectively. Since these absorption bands were not observed in the spectra of the as-synthesized nanozeolites, this provided strong evidence for the effective surface modification of the nanozeolite surfaces [52,59–62].

Absorption bands related to the APTMS, such as that for (C—N) of the aminopropyl group, typically observed at wavelengths between 1000 and 1200 cm^{-1}, could not be unequivocally assigned, due to the overlap of T—O—T bond absorption bands. Similarly, bands corresponding to stretching of amino group N—H, at around 3300 cm^{-1}, overlapped with the strong absorption bands of water molecules and silanol groups in the region 3000–3600 cm^{-1} [63].

Electrostatic interaction plays a significant role in enzyme immobilization. Therefore, in order to gain a better understanding of the role of organic modification of the nanozeolite surface and its influence on the overall immobilization process, zeta potential determinations were performed for the as-synthesized nanozeolites, the APTMS-functionalized nanozeolites, the APTMS/GA-functionalized nanozeolites, and the APTMS/Lipase and APTMS/GA/Lipase complexes.

Negative zeta potential values were found for U-Nano/TS1 (−34.4 mV), U-Nano/GIS (−39.8 mV), U-Nano/LTA (−49.8 mV), U-Nano/BEA (−25.1 mV), and U-Nano-X/Na (−38.2 mV) (Fig. 4). Since the *Thermomyces lanuginosus* enzyme is also negatively charged, the repulsive forces resulted in significantly smaller amounts of immobilized enzymes, compared to the nanozeolites functionalized with APTMS and GA (Table 3) [58,64]. The zeta potentials for the nanozeolites functionalized with APTMS and APTMS/GA (Fig. 4) revealed that the surfaces of these zeolite were positively charged: N-Nano/TS1 (19.6 mV), N-Nano/GIS (3.8 mV), N-Nano/LTA (17.6 mV), N-Nano/BEA (24.1 mV), N-Nano/X (21.6 mV), N-Nano/X/Ni (21.6 mV), NG-Nano/TS1(30.2 mV), NG-Nano/GIS (25.8 mV), NG-Nano/LTA (23.7 mV), NG-Nano/BEA (37.8 mV), NG-Nano/X (28.2 mV), and NG-Nano-X/Ni (45.6 mV). After immobilization, all the nanozeolite-enzyme complexes presented negative zeta potential values (Supplementary materials section). The positively charged surfaces affected the amounts of immobilized enzyme, and it was also observed that the enzymatic activities were higher for enzyme immobilized on the functionalized supports (Table 3). A possible explanation for this enhancement of enzymatic activity could be related to the generation of spacer arms between the enzyme and the supports, leading to an increase in the immobilized enzyme concentration promoted by the reactive organic chemical groups of the APTMS and GA molecules.

Table 3
The amount of Thermomyces lanuginosus lipase immobilized on the zeolitic supports, their enzymatic activity after immobilization and the transesterification reactions of microalgae oil to produce biodiesel. U-(unfunctionalized support), N-(APTMS funcionalized support), NG-(APTMS-Glutaraldehyde functionalized support).

Nanozeolite	Immobilization (%)	Enzymatic activity (U/mg-support)	Ethyl esters (%)
U-Nano-TS1	31.9	15.6	12.9
N-Nano-TS1	97.6	48.0	56.6
NG-Nano-TS1	98.5	56.0	55.6
U-Nano-GIS	15.2	4.0	7.2
N-Nano-GIS	30.2	56.0	48.1
NG-Nano-GIS	79.1	28.0	60.3
U-Nano-LTA	18.4	8.0	7.7
N-Nano-LTA	97.1	68.0	89.8
NG-Nano-LTA	100	46.0	44.9
U-Nano-BEA	16.9	3.6	21.6
N-Nano-BEA	100	76.4	92.7
NG-Nano-BEA	100	68.0	67.7
U-Nano-X	18.3	2.0	17.8
N-Nano-X	76.6	74.0	94.6
NG-Nano-X	98.0	56.0	71.6
U-Nano-X/Ni	43.7	64.0	94.0
N-Nano-X/Ni	95.6	76.0	93.4
NG-Nano-X/Ni	97.7	78.0	93.0

According to the proposed mechanism, enzyme immobilization occurred at a greater distance from the support microenvironment, which could help to avoid distortions of the enzyme structure and enhance exposure of the active sites to the substrate, hence facilitating enzyme/substrate contact and optimizing mass transfer in the system [65–70].

Systematic catalytic studies of the transesterification reactions of microalgae oil to produce biodiesel using the different nanozeolite-enzyme complexes were performed using the following supports: a) unfunctionalized supports (U-Nano/TS1-TLL, U-Nano/GIS-TLL, U-Nano/LTA-TLL, U-Nano/BEA-TLL, U-Nano/X-TLL, and U-Nano-X/Ni-TLL); b) amine-terminated surface supports (N-Nano/TS1-TLL, N-Nano/GIS-TLL, N-Nano/LTA-TLL, N-Nano/BEA-TLL, N-Nano/X-TLL, and N-Nano-X/Ni-TLL); and c) glutaraldehyde crosslinked amine-terminated surface supports (NG-Nano/TS1-

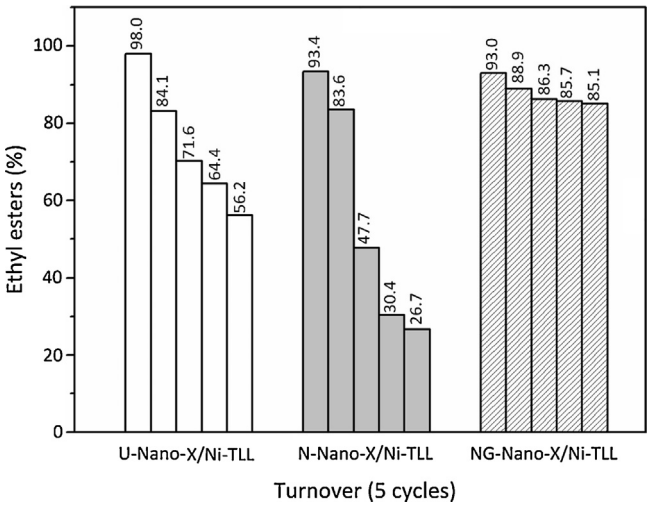

Fig. 5. Turnover for the U-Nano-X/Ni-TLL,N-Nano-X/Ni-TLL and NG-Nano-X/Ni-TLL complexes.

TLL, NG-Nano/GIS-TLL, NG-Nano/LTA-TLL, NG-Nano/BEA-TLL, NG-Nano/X-TLL, and NG-Nano-X/Ni-TLL). The FAEEs yields of all the reactions were determined by gas chromatography analysis (Table 3).

The experimental reaction conditions were standardized in order to compare the performances of the three catalyst groups. The FAEEs yields obtained for all the functionalized nanozeolitic supports were superior to those for the unfunctionalized zeolites (Table 3). For N-Nano/TS1-TLL and NG-Nano/TS1-TLL, the FAEEs yields (56.6 and 55.6%, respectively) were approximately 4-fold higher than the yield obtained using the unfunctionalized U-Nano/TS1-TLL support (12.9%) (Table 3).

The FAEEs yields achieved with the nanozeolite-enzyme complexes N-Nano/LTA-TLL (89.8%), N-Nano/BEA-TLL (92.7%),and N-Nano/X-TLL (94.6%) were higher than obtainedwith the NG-Nano/LTA-TLL (44.9%), NG-Nano/BEA-TLL (67.5%),and NG-Nano-X-TLL (71.6%) complexes (Table 3). A possible explanation for the lower FAEEs yields observed for the NG supports was distortion of the enzyme structure caused by reticulation of the glutaraldehyde molecules with the enzyme amino groups, which consequently reduced access of the substrate to the specific catalytic site of the enzyme [42,43].

One exception was observed among the Nano/GIS derivative supports. The FAEEs yield for the N-Nano/GIS-TLL complex (48.1%) was lower than for the NG-Nano/GIS-TLL complex (60.3%). Possible explanations for this include low dispersibility of the biocatalyst in the reaction solution, or the low amount of the enzyme immobilized on this support (30.2%).

High FAEEs yields were observed for the U-Nano-X/Ni-TLL (94.0%), N-Nano-X/Ni-TLL (93.4%), and NG-Nano-X/Ni-TLL (93.0%) complexes (Table 3). A graphical representation of all the transesterification results is provided in the Supplementary materials section. Reuse experiments were therefore performed using these nanozeolite-enzyme complexes (Fig. 5). The important role played by nickel in enzyme immobilization and enzymatic activity has been reported previously [44,71] and was also observed here for the nanozeolite supports ion-exchanged with nickel.

The FAEEs yield obtained with the U-Nano-X/Ni-TLL complex decreased from 98 to 56.2% after five cycles of reuse in the reaction, while the N-Nano-X/Ni-TLL complex showed a sharp decrease of the FAEEs yield from 93.4 to 26.7%. The NG-Nano-X/Ni-TLL complex presented the smallest decrease (from 93 to 85.1%) in the FAEEs yield. The highest decrease observed for N-Nano-X/Ni-TLL could in principle be attributed to the weak interactions between the APTMS amino groups and the enzyme, which could lead to the leaching or desorption of large amounts of the lipase from the solid during the successive reuses.

The excellent performance shown by NG-Nano-X/Ni-TLL in the reuse experiments (Fig. 5) demonstrated the potential of the complex as a suitable biocatalyst for biofuel production reactions in long-term continuous systems, due to the fact that the immobilized enzyme was covalently bonded to the support, resulting in a more stable biocatalyst. The chemical functionalization of the Nano-X/Ni surfaces with APTMS and glutaraldehyde enhanced the hydrophobicity of the biocatalyst, hence decreasing glycerol adsorption in the biocatalyst microenvironment and avoiding deactivation of the enzyme active sites [42,43].

4. Conclusions

- Nanozeolite surfaces chemically functionalized with APTMS and the glutaraldehyde crosslinking agent were efficient solid matrices for *T. lanuginosus* lipase immobilization;
- Functionalization of the nanozeolite surfaces enhanced the amount of immobilized enzyme and increased the enzymatic activity, compared to unfunctionalized nanozeolitic supports;
- Nanozeolite-enzyme complexes prepared with supports that had been previously chemically functionalized were more efficient biocatalysts in the transesterification reaction of microalgae oil to produce biodiesel, achieving high FAEEs yields;
- The catalytic performances of biocatalysts prepared with unfunctionalized nanozeolitic supports were very poor, compared to the use of functionalized supports;
- Although all the nanozeolite-enzyme complexes (U-Nanozeolite, N-Nanozeolite, and NG-Nanozeolite) were able to catalyze the transesterification of microalgae oil into biodiesel (FAEEs), the best catalytic performances were obtained with the complexes produced using nanozeolitic supports previously ion-exchanged with nickel (U-Nano-X/Ni-TLL, N-Nano-X/Ni-TLL, and NG-Nano-X/Ni-TLL).
- In reuse experiments with the biocatalysts, the best results were obtained with NG-Nano-X/Ni-TLL, where the enzyme was covalently bonded to the nanozeolitic support. The NG-Nano-X/Ni-TLL complex showed excellent potential for use as a suitable biocatalyst for biofuel production in long-term continuous system reactions.

Acknowledgments

Financial support for this ongoing research project is provided by the São Paulo State Research Foundation (FAPESP), in the form of a scientific award to JGN (grant #11/51851-5), and by CNPq (grants #465594/2014-0 and #406761/2013-2). AV (grant #11/10092-4) and AHM (grant #2016/24303-0) thank FAPESP for fellowships. We thank Dr. Marcia Cabrera for allowing us to use the zeta potential instrument (FAPESP grant #2012/24259-0). We appreciate the assistance of Dr. Carlos A. O. Ramirez, Dr. Carlos A. Costa, and Dr. Evandro Lanzoni (Brazilian National Laboratory of Nanotechnology – LNNano) in the SEM-FEG and AFM microscopy experiments.

Appendix A. Supplementary data

Supplementary data associated with this article can be found, in the online version, at https://doi.org/10.1016/j.colsurfb.2018.02.029.

References

[1] F.R. Ma, M.A. Hanna, Bioresour. Technol. 70 (1999) 1–15.
[2] A. Corma, S. Iborra, A. Velty, Chem. Rev. 107 (2007) 2411–2502.

[3] S.N. Naik, V.V. Goud, P.K. Rout, A.K. Dalai, Renew. Sustain. Energy Rev. 14 (2010) 578–597.
[4] A.L. Ahmad, N.H.M. Yasin, C.J.C. Derek, J.K. Lim, Renew. Sustain. Energy Rev. 15 (2011) 584–593.
[5] E.F. Aransiola, T.V. Ojumu, O.O. Oyekola, T.F. Madzimbamuto, D.I.O. Ikhu-Omoregbe, Biomass Bioenergy 61 (2014) 276–297.
[6] M. Balat, Energy Convers. Manage. 52 (2011) 1479–1492.
[7] P.S. Nigam, A. Singh, Prog. Energy Combust. Sci. 37 (2011) 52–68.
[8] T.M.Y. Khan, A.E. Atabani, I.A. Badruddin, A. Badarudin, M.S. Khayoon, S. Triwahyono, Renew. Sustain. Energy Rev. 37 (2014) 840–851.
[9] J.W. Goodrum, D.P. Geller, T.T. Adams, Biomass Bioenergy 24 (2003) 249–256.
[10] M.E. da Cunha, Fuel Process. Technol. 90 (2009) 570–575.
[11] P. Felizardo, M.J. Neiva Correia, I. Raposo, J.F. Mendes, R. Berkemeier, J.M. Bordado, Waste Manage. 26 (2006) 487–494.
[12] A.N. Phan, T.M. Phan, Fuel 87 (2008) 3490–3496.
[13] S.P. Singh, D. Singh, Renew. Sustain. Energy Rev. 14 (2010) 200–216.
[14] M.G. Kulkarni, A.K. Dalai, Ind. Eng. Chem. Res. 45 (2006) 2901–2913.
[15] T.M. Mata, A.A. Martins, N.S. Caetano, Renew. Sustain. Energy Rev. 14 (2010) 217–232.
[16] D.-T. Tran, C.-L. Chen, J.-S. Chang, Bioresour. Technol. 135 (2013) 213–221.
[17] M. Fatih Demirbas, Appl. Energy 86 (2009) 151–161.
[18] A. Tabernero, E.M. Martín del Valle, M.A. Galán, Biochem. Eng. J. 63 (2012) 104–115.
[19] X. Miao, Q. Wu, Bioresour. Technol. 97 (2006) 841–846.
[20] T. Taparia, M. Mvss, R. Mehrotra, P. Shukla, S. Mehrotra, Biotechnol. Appl. Biochem. 63 (2016) 715–726.
[21] D.E. Trimbur, C.S. Im, H.F. Dillon, A.G. Day, S. Franklin, A. Coragliotti, Google Patents, 2013.
[22] H. Xu, X. Miao, Q. Wu, J. Biotechnol. 126 (2006) 499–507.
[23] X. Wu, R. Ruan, Z. Du, Y. Liu, Energies 5 (2012) 2667–2682.
[24] Y.C. Sharma, B. Singh, Renew. Sust. Energ. Rev. 13 (2009) 1646–1651.
[25] L. Fjerbaek, K.V. Christensen, B. Norddahl, Biotechnol. Bioeng. 102 (2009) 1298–1315.
[26] M. Di Serio, R. Tesser, L. Pengmei, E. Santacesaria, Energy Fuels 22 (2008) 207–217.
[27] E. Lotero, Y. Liu, D.E. Lopez, K. Suwannakarn, D.A. Bruce, J.G. Goodwin, Ind. Eng. Chem. Res. 44 (2005) 5353–5363.
[28] F. Yagiz, D. Kazan, A.N. Akin, Chem. Eng. J. 134 (2007) 262–267.
[29] X. Fan, Lipid Technol. 24 (2012) 31–32.
[30] M. Szczesna-Antczak, A. Kubiak, T. Antczak, S. Bielecki, Renew. Energy 34 (2009) 1185–1194.
[31] T. Tan, J. Lu, K. Nie, L. Deng, F. Wang, Biotechnol. Adv. 28 (2010) 628–634.
[32] A. Bajaj, P. Lohan, P.N. Jha, R. Mehrotra, J. Mol. Catal. B: Enzym. 62 (2010) 9–14.
[33] C. Mateo, J.M. Palomo, G. Fernandez-Lorente, J.M. Guisan, R. Fernandez-Lafuente, Enzyme Microb. Technol. 40 (2007) 1451–1463.
[34] G.J. Suppes, M.A. Dasari, E.J. Doskocil, P.J. Mankidy, M.J. Goff, Appl. Catal. A 257 (2004) 213–223.
[35] M.J. Ramos, A. Casas, L. Rodríguez, R. Romero, Á. Pérez, Appl. Catal. A: Gen. 346 (2008) 79–85.
[36] H. Fukuda, A. Kondo, H. Noda, J. Biosci. Bioeng. 92 (2001) 405–416.
[37] H.T. Hwang, et al., Biotechnol. Bioeng. 111 (2014) 639–653.
[38] A. Macario, et al., Biocatal. Biotransform. 25 (2007) 328–335.
[39] A. Macario, et al., Stud. Surf. Sci. Catal. 155 (2005) 381–394.
[40] F.N. Serralha, et al., J. Mol. Catal. B: Enzym. 4 (1998) 303–311.
[41] A. de Vasconcellos, Microporous Mesoporous Mater. 163 (2012) 343–355.
[42] S. Mitchell, J. Pérez-Ramírez, Catal. Today 168 (2011) 28–37.
[43] P. Zucca, E. Sanjust, Molecules 19 (2014) 14139–14194.
[44] A. de Vasconcellos, Microporous Mesoporous Mater. 214 (2015) 166–180.
[45] C.S. Cundy, J.O. Forrest, R.J. Plaisted, Microporous Mesoporous Mater. 66 (2003) 143–156.
[46] J. Kecht, B. Mihailova, K. Karaghiosoff, S. Mintova, T. Bein, Langmuir 20 (2004) 5271–5276.
[47] O. Larlus, S. Mintova, S.T. Wilson, R.R. Willis, H. Abrevaya, T. Bein, Microporous Mesoporous Mater. 142 (2011) 17–25.
[48] E. Biemmi, T. Bein, Langmuir 24 (2008) 11196–11202.
[49] B.Z. Zhan, M.A. White, K.N. Robertson, T.S. Cameron, M. Gharghouri, Chem. Commun. 13 (2001) 1176–1177.
[50] E.P. Plueddemann, Addit. Plast. 1 (1978) 123–167.
[51] Y. Li, H.-M. Guan, T.-S. Chung, S. Kulprathipanja, J. Memb. Sci. 275 (2006) 17–28.
[52] D. Jung, M. Hartmann, Stud. Surf. Sci. Catal. 174 (2008) 1045–1050.
[53] K.S. Yang, J.-H. Sohn, H.K. Kim, J. Biosci. Bioeng. 107 (2009) 599–604.
[54] C.S. Cundy, J.O. Forrest, Microporous Mesoporous Mater. 72 (2004) 67–80.
[55] H. Faghihian, M. Moayed, A. Firooz, M. Iravani, J. Colloid Interface Sci. 393 (2013) 445–451.
[56] B.Z. Zhan, et al., Chem. Mater. 14 (2002) 3636–3642.
[57] E.M. Flaningen, in: J.A. Rabo (Ed.), Zeolite Chemistry and Catalysis, ACS, Washington, 1979, p. 80.
[58] H. Wang, W. Zhang, F. Zhang, Y. Cao, W. Su, J. Magn. Magn. Mater. 320 (2008) 1916–1920.
[59] A.E. David, N.S. Wang, V.C. Yang, A.J. Yang, J. Biotechnol. 125 (2006) 395–407.
[60] J.H. Chen, Q.L. Liu, X.H. Zhang, Q.G. Zhang, J. Membr. Sci. 292 (2007) 125–132.
[61] M.C. Chang, J. Tanaka, Biomaterials 23 (2002) 4811–4818.
[62] H.S. Mansur, C.M. Sadahira, A.N. Souza, A.A.P. Mansur, Mater. Sci. Eng. C 28 (2008) 539–548.
[63] C.-H. Chiang, H. Ishida, J.L. Koenig, J. Colloid Interface Sci. 74 (1980) 396–404.
[64] F. Bucatariu, C.-A. Ghiorghita, F. Simon, C. Bellmann, E.S. Dragan, Appl. Surf. Sci. 280 (2013) 812–819.
[65] K. Min, J. Kim, K. Park, Y.J. Yoo, J. Mol. Catal. B: Enzym. 83 (2012) 87–93.
[66] H. Rong, Y. Xiaogang, S. Jun, G. Feng, P. Bifeng, C. Daxiang, Nanotechnology 18 (2007) 315601.
[67] W.S. Adriano, E.H.C. Filho, J.A. Silva, R.L.C. Giordano, L.R.B. Gonçalves, Braz. J. Chem. Eng. 22 (2005) 529–538.
[68] Ö. Alptekin, S. Seyhan Tükel, D. Yildirim, D. Alagöz, Enzyme Microb. Technol. 49 (2011) 547–554.
[69] J.N. Talbert, J.M. Goddard, Colloids Surf. B Biointerfaces 93 (2012) 8–19.
[70] X. Feng, D.A. Patterson, M. Balaban, E.A.C. Emanuelsson, Colloids Surf. B Biointerfaces 102 (2013) 526–533.
[71] Z. Wu, W. Qi, M. Wang, R. Su, Z. He, J. Mol. Catal. B: Enzym. 110 (2014) 32–38.